Research Article Vol. 31, No. 25 / 4 Dec 2023 / Optics Express 42723
Optics EXPRESS

Orthogonal spatial coding with stimulated parametric down-conversion

YANG XU,[1,*] SIRUI TANG,[2] A. NICHOLAS BLACK,[1] AND ROBERT W. BOYD[1,2,3]

[1]Department of Physics and Astronomy, University of Rochester, Rochester, New York 14627, USA
[2]The Institute of Optics, University of Rochester, Rochester, New York 14627, USA
[3]Department of Physics, University of Ottawa, Ottawa, Ontario K1N 6N5, Canada
[*]yxu100@ur.rochester.edu

Abstract: Orthogonal optical coding is widely used in classical multi-user communication networks. Using the phase conjugation property of stimulated parametric down-conversion, we extend the current time-domain orthogonal optical coding scheme to the spatial domain to encode and decode image information. In this process, the idler beam inherits the complex conjugate of the field information encoded in the seed beam. An encoding phase mask introduced onto the input seed beam blurs the image transferred to the idler. The original image is restored by passing the coded transferred image through a corrective phase mask placed in the momentum space of the idler beam. We expect that this scheme can also inspire new techniques in secure image transmission, aberration cancellation, and frequency conversion imaging.

1. Introduction

The conventional physical realization of the orthogonal coding protocol is the spectral coding of coherent optical pulses [1–3], where the sender encodes the message with a randomly generated code to one half of the spectrum, and only the receiver who applies the correct code to the opposite half can retrieve the image from the noise. Recently, a quantum version of orthogonal spectral coding [3] was also realized with the correlation of entangled photons in the time domain.

The fast development in remote sensing and detection urgently calls for a reliable coding protocol for the exchange of image information. In the spatial domain, wavefront aberrations often degrade the image quality in both classical and quantum imaging schemes. In particular, quantum imaging schemes [4,5] are highly vulnerable to aberrations because the correlated photon pairs produced in the spontaneous parametric down-conversion (SPDC) become disentangled even under very small perturbations. Despite the destructive nature of wavefront aberrations in imaging systems, the phase mask in the Fourier plane that leads to aberrations can be used to encode and secure image information. This suggests that a coding protocol of image transfer in the spatial domain should be possible in principle if wavefront aberrations can be effectively canceled. Recently, multiple schemes have been demonstrated to correct the wavefront aberrations [6] in quantum imaging experiments. Both local aberration cancellations [7,8] and nonlocal cancellations [9] which use the position-momentum entangled photon pairs produced in a spontaneous parametric down-conversion have been performed experimentally.

In this letter, we extend the latest nonlocal aberration cancellation scheme [9] to a non-degenerate case and demonstrate an orthogonal optical coding scheme using the spatial correlation of the seed-idler pair in a stimulated parametric down-conversion. Recent theoretical work [10] has demonstrated that stimulated parametric down-conversion, also known as the difference frequency generation (DFG), provides a more efficient method to extract the same information as by using a photon pair produced by its quantum counterparts – SPDC [11]. This close connection between DFG and SPDC has initiated a number of new methods that are more efficient to characterize and harness the spatial correlation of photon pairs [12,13]. Taking advantage of the high photon flux

#506383 https://doi.org/10.1364/OE.506383
Journal © 2023 Received 21 Sep 2023; revised 1 Nov 2023; accepted 21 Nov 2023; published 1 Dec 2023

Optics EXPRESS

in the seeded process, we show that a practical image coding scheme using the spatial correlation of photon pairs can be realized through DFG.

2. Principle of orthogonal spatial coding

In a DFG process, the seed beam $\mathbf{E}_s$ and the pump beam $\mathbf{E}_p$ are mixed in a nonlinear crystal and generate a third beam $\mathbf{E}_i$, which we call the idler beam. Each field has a transverse spatial profile $\mathcal{E}_j(\mathbf{r})$ $(j = p, i, s)$:

$$\mathbf{E}_j = \mathcal{E}_j(\mathbf{r})e^{ik_j z}\mathbf{e}_j \tag{1}$$

where $\mathbf{e}_j (j = p, i, s)$ is the unit polarization vector. The process satisfies energy conservation $\omega_p - \omega_s = \omega_i$ and momentum conservation $\mathbf{k}_p - \mathbf{k}_s = \mathbf{k}_i$. Assuming that the pump is undepleted by the nonlinear interaction and the process is perfectly phase-matched, the coupled-amplitude equations describing the DFG are given by [14]

$$\frac{d\mathcal{E}_i}{dz} = \frac{2id_{\text{eff}}\omega_i^2}{k_i c^2}\mathcal{E}_p\mathcal{E}_s^* \tag{2}$$

$$\frac{d\mathcal{E}_s}{dz} = \frac{2id_{\text{eff}}\omega_s^2}{k_s c^2}\mathcal{E}_p\mathcal{E}_i^* \tag{3}$$

where $d_{\text{eff}} = \frac{1}{2}\chi^{(2)}$ describes the second-order nonlinearity of the crystal. In the thin-crystal limit, the spatial profile of the down-converted idler beam obtained from Eq. (2) and Eq. (3) is proportional to the product of the pump beam spatial profile and the conjugate of the seed beam spatial profile [15]:

$$\mathcal{E}_i(\mathbf{r}) \propto \mathcal{E}_p(\mathbf{r})\mathcal{E}_s^*(\mathbf{r}) \tag{4}$$

The code used to code the image is described by a momentum-dependent phase factor $e^{i\phi_s(\mathbf{k}_s)}$ acting on the angular spectrum of the seed beam that carries the image:

$$\widetilde{\mathcal{E}}_s(\mathbf{k}_s) = \widetilde{\mathcal{E}}_{s,\text{message}}(\mathbf{k}_s)e^{i\phi_s(\mathbf{k}_s)} \tag{5}$$

where $\widetilde{\mathcal{E}}_{s,\text{message}}(\mathbf{k}_s)$ is the angular spectrum of the image message encoded in the seed beam.

Using the property given by Eq. (4), we can express the angular spectrum of the down-converted idler beam as

$$\widetilde{\mathcal{E}}_i(\mathbf{k}_i) \propto \widetilde{\mathcal{E}}_p(\mathbf{k}_p) * \widetilde{\mathcal{E}}_{s,\text{message}}^*(\mathbf{k}_s)e^{-i\phi_s(\mathbf{k}_s)} \tag{6}$$

where $\widetilde{\mathcal{E}}_p(\mathbf{k}_p)$ is the angular spectrum of the pump wave and $*$ is the convolution operator. Thus, under the plane-wave-pump approximation, $\mathbf{k}_p = \mathbf{k}_i + \mathbf{k}_s \approx 0$, we are able to completely filter the effect of the encoding aberrations by placing a momentum-dependent phase mask $\phi_i(\mathbf{k}_i) = \phi_s(-\mathbf{k}_s)$ at the Fourier plane of the idler arm.

To implement orthogonal spectral coding in the spatial domain, we apply a spatial code matrix to the angular spectrum of the image we want to send. That is, we introduce artificial random aberrations by passing the Fourier transform of the image through an encoding phase mask. The phase mask takes the form of an $N \times N$ matrix for which each element is randomly chosen from two values, 0 and π. The receiver only measures a randomly distorted image without a matching decoding phase mask.

3. Experimental results

In our experiment, the spatial code is generated by a random phase mask on a spatial light modulator (SLM) placed at the Fourier plane of the seed beam.We first create an $N \times N$ matrix (N<1000) where each entry ϕ_{ij}^{rand} takes a value of either 0 or π. This procedure provides the spatial code we use to encode the image transferred to the receiver (Fig. 1). Then we expand

Optics EXPRESS

the $N \times N$ matrix to fill the entire SLM window using a bicubic interpolation method [16] to ensure the smooth phase change across the phase mask printed on the SLM. This resulting phase profile $\phi^{\text{rand}}(x, y)$ is used on both SLMs to introduce and cancel the effect of the spatial coding in the system. Due to the momentum anticorrelation between the idler and the seed, the decoding phase mask printed on the SLM in the idler beam should be a flipped copy of the phase mask on the SLM that encodes the image on the seed beam. This means the random phase profile printed on the SLM in the idler arm should satisfy $\phi^{\text{rand}}(x_i, y_i) = \phi^{\text{rand}}(-x_s, -y_s)$ where (x_n, y_n) $(n = i, s)$ is the pixel coordinate of the SLM screen in the idler/signal beam.

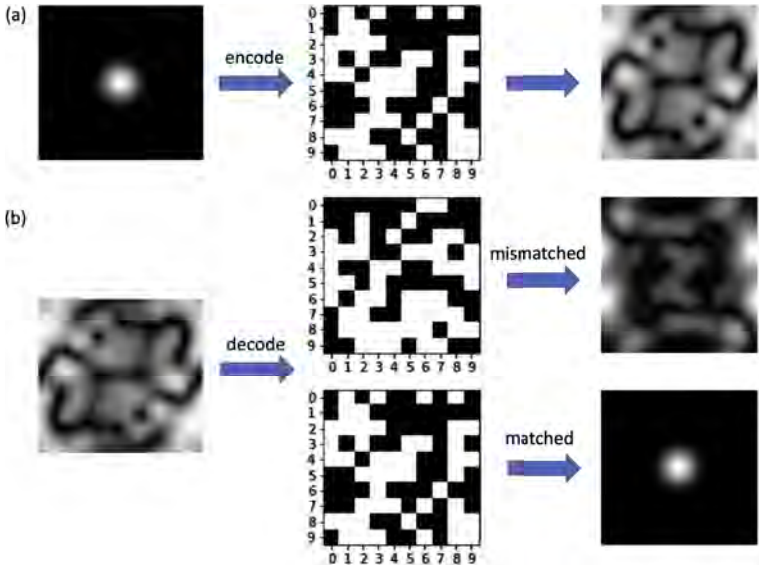

Fig. 1. Principle of orthogonal spatial coding. (a) Encoding an image. A random matrix of 0 and π phase shifts is applied to the Fourier transform of the image sent to the receiver. The encoding phase mask introduces artificial aberrations to the image and produces a distorted and blurry image at the receiver's end. For clarity and simplicity, the image sent here is a simple Gaussian beam and the size of the encoding matrix is chosen to be 10×10. (b) Decoding the transferred pattern. The Gaussian beam is recovered when the receiver applies a matching phase mask. Any other phase masks keep the image distorted and blurry.

Figure 2 shows the experimental setup used to implement the orthogonal spatial coding of images with DFG. A Type-II beta barium borate (BBO) nonlinear crystal was pumped by a horizontally polarized, 20 mW, c.w. 405 nm collimated Gaussian beam with a diameter of 1.7 mm produced by a diode laser. The seed beam with a wavelength of 780 nm was first collimated and then illuminated an object that features the USAF 1951 target. Both the pump and the seed beam were spectrally filtered with a narrowband filter (10 nm) centered at 405 nm and 780 nm respectively. A half-wave plate was placed after each narrowband spectral filter to control the polarization of the pump and the signal beam so that the phase-matching condition of the nonlinear frequency conversion is satisfied. The object, illuminated by the 780 nm seed beam, was imaged onto the Type-II BBO nonlinear crystal by a $4f$ (f = 20 cm) image-relay system. A spatial light modulator (Meadowlark E-series 1920×1200 SLM) was used to introduce the encoding key to the image in the seed beam. The image is encoded by the random phase mask printed on the SLM placed in the Fourier plane of the seed beam. The DFG process between the pump beam and seed beam is observed when the phase-matching condition is satisfied. The encoded conjugate image is transferred to the idler beam whose wavelength is 842 nm. Another $4f$ system (f = 20cm) relays the conjugate image produced in the DFG onto an ICCD camera. A

Optics EXPRESS

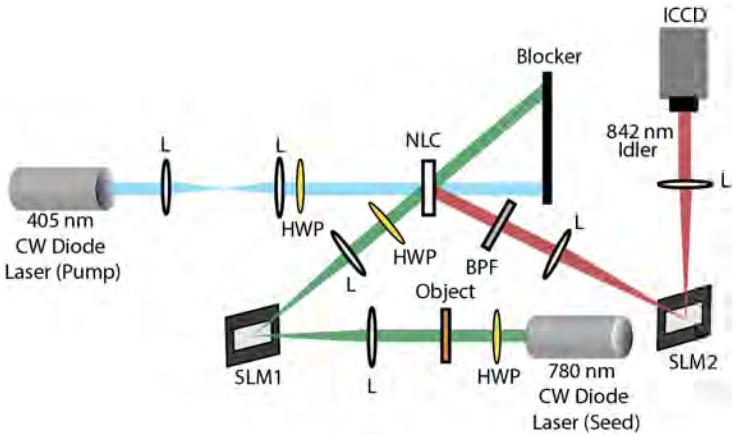

Fig. 2. Schematic of the experimental setup. L: lens; HWP: half-wave plate; BPF: band-pass filter; NLC: Type-II nonlinear crystal (BBO). A Type-II BBO crystal is pumped by a 405nm CW laser beam with a Gaussian spatial profile (drawn in blue). The seed beam (drawn in green) passes through the object in the form of the USAF test chart. The image is then encoded by the random pattern imposed on SLM1. The encoded image, which is imaged onto the BBO crystal, seeds the DFG process. The phase mask on SLM2 recovers the image transferred to the idler beam (drawn in red).

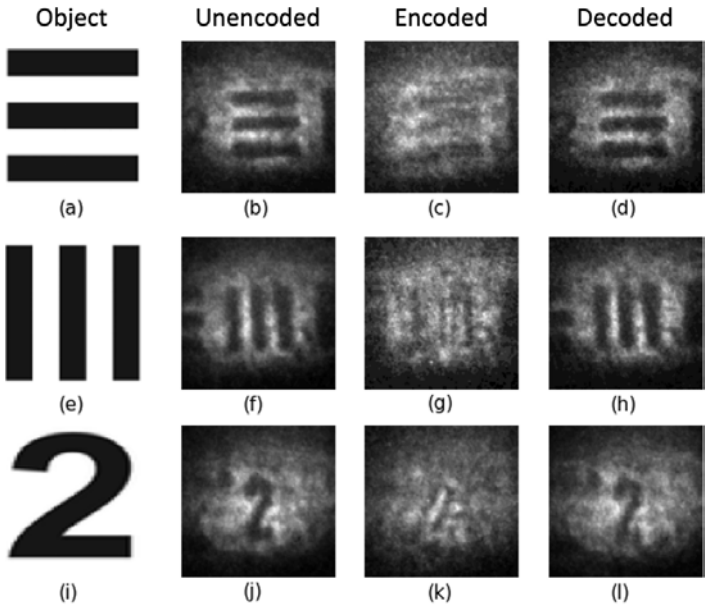

Fig. 3. Air-force target and images captured by the ICCD camera. (a,e,i): objects on the USAF 1951 chart (b-d): the unencoded image, encoded image, and decoded image of three horizontal bars transferred to the idler beam at 842 nm; (f-h):the unencoded image, encoded image, and decoded image of three vertical bars transferred to the idler beam at 842 nm; (j-l): the unencoded image, encoded image, and decoded image of the digit "2" transferred to the idler beam at 842 nm.

second spatial light modulator (Santec SLM-200) was placed at the Fourier plane of the idler beam to decode the transferred conjugate image.

Optics EXPRESS

We transferred three different objects, three horizontal bars, three vertical bars, and the digit "2" on the USAF 1951 target with our image coding setup. The down-converted idler beam spans around 2.4mm in width and around 1.6mm in height. Figure 3(b), 3(f), and 3(j) show the images of the objects transferred onto the 842 nm idler beam when the encoding phase mask is turned off. Figure 3(c), 3(g), and 3(k) show the distorted images collected on the ICCD camera when a random phase mask, $\phi_i(\mathbf{k}_i)$, is applied to the image in the seed beam. The phase value on the SLM in the idler arm is set to zero everywhere so that no decoding is made. Figure 3(d), 3(h) and 3(l) show the recovered images when the correct decoding phase mask, $\phi_i(\mathbf{k}_i) = \phi_s(-\mathbf{k}_s)$, is printed on the SLM in the idler arm. In all the images collected by the ICCD camera, we can observe some minor discrepancies from the original USAF 1951 target images, even in the transferred images without encoding. This is because the angular spectrum of the pump beam is approximately a Gaussian distribution with a small but non-zero width, which is only a reasonable approximation to a Dirac delta function. According to Eq. (6), this difference leads to a minor deviation from the original target image in the down-converted idler beam even without encoding.

4. Discussion

To quantify the effect of the encoding and decoding phase masks, we use the Pearson correlation coefficient (PCC) [17] to describe the degree of similarity between two images. We take the USAF 1951 target images as benchmarks and calculate the Pearson correlation coefficients for the transferred image without aberrations, the decoded image, and the decoded image in the 842-nm idler beam respectively. We first standardize all images collected and the target images by converting them into 100×100 8-bit-grayscale form. Then we define the Pearson correlation coefficient r that quantifies the deviation from the target in the following way [18]:

$$r = \frac{\sum_{i,j=1}^{N}(x_{ij} - m_x)(y_{ij}^{\text{targ}} - m_y^{\text{targ}})}{\sqrt{\sum_{i,j=1}^{N}(x_{ij} - m_x)^2 \sum_{i,j=1}^{N}\left(y_{ij}^{\text{targ}} - m_y^{\text{targ}}\right)^2}} \tag{7}$$

where x_{ij} (y_{ij}^{targ}) is the 8-bit grayscale value of the pixel in the i-th row and j-th column of the image tested (target object), and m_x (m_y^{targ}) is the mean grayscale value of all pixels in the image tested (target object). The absolute value of the Pearson correlation coefficient, r, ranges from 0 to 1. If $|r| = 1$, this means the image collected by the ICCD and the target image are fully correlated or anti-correlated, so all features in the target are honestly reproduced. If $|r| = 0$, this means the image collected by the ICCD camera and the target image have no correlation. In this case, no information about the target can be obtained from the image collected by the ICCD camera.

Table 1 shows the Pearson correlation coefficients (PCC) calculated for all three features on the USAF 1951 target. For transferred images and decoded images, the average PCC's are 0.627 and 0.598 respectively, showing a strong correlation with the original target images. On the contrary, the average PCC of encoded images is 0.212. Considering the common white background in all images, this value shows a minimal similarity between the encoded images and target images. Overall, the results shown in Fig. 3 and Table 1 indicate that the coded image can be effectively transferred and restored through a non-degenerate stimulated parametric down-conversion process as expected.

Optics EXPRESS

Table 1. Pearson correlation coefficients(PCC). PCC calculated here describes the correlation between the image collected by the ICCD camera and the objects on the USAF 1951 target. A larger value stands for a stronger correlation between the image tested and the object. Note that the PCC of the decoded image of horizontal/vertical bars is slightly higher than the unencoded image due to the simplicity of the target. For more complicated geometries like the digit "2", the correlation to the ground truth of the unencoded image exceeds the decoded image as expected.

	Horizontal Bars	Vertical Bars	Digit "2"
Unencoded	0.682	0.666	0.535
Encoded	0.328	0.211	0.0962
Decoded	0.695	0.674	0.454

5. Conclusion and outlook

In our orthogonal spatial coding scheme, the color of the received image is different from the image sent out in the seed beam. Therefore, we expect that, with proper modifications in our setup, our image coding setup may also find a suitable place in many frequency-conversion imaging schemes [19,20]. In these experiments, the photon interacting with the sample is up or down converted into a different wavelength before it is collected by the detector because direct observation of samples under UV or visible light often induces fluorescence [21], and a long exposure of the biological samples to high-frequency electromagnetic radiation can also cause sample photodamage and phototoxicity [22]. The orthogonal spatial coding technique used in this letter may suggest new possibilities to correct image aberrations caused by anisotropy and optical defects in biological samples in many frequency-conversion imaging applications. Our spatial encoding scheme also paves the way for developing a secure long-distance quantum communication protocol. The wavelength of the information-carrying signal compatible with the current long-distance fiber-based communication infrastructure can be translated to a shorter wavelength compatible with the current silicon-based single-photon detectors [23].

In conclusion, we have proposed and demonstrated an orthogonal spatial coding scheme based on classical difference frequency generation. In the low-gain regime, the output field of the stimulated parametric down-conversion is proportional to the product of the pump field and the conjugate of the seed field. Making use of this property, our experiment has shown that the encoded image in the seed beam can be transferred to the idler beam at a different wavelength. The distorted image transferred to the idler beam can be recovered by canceling the effect of the spatial coding with a proper corrective phase mask placed at the Fourier plane of the idler. We expect that the scheme proposed in this letter can be further developed into several practical frequency-conversion imaging schemes in aberrating media.

Funding. Office of Naval Research (N00014-19-1-2247); Office of Science (FWP 762954); Government of Canada; Natural Sciences and Engineering Research Council of Canada; Canada Research Chairs; Canada First Research Excellence Fund.

Acknowledgments. The authors thank Saumya Choudhary and Saleem Iqbal for useful discussions.

Disclosures. The authors declare no conflicts of interest.

Data availability. Data underlying the results presented in this paper are not publicly available at this time but may be obtained from the authors upon reasonable request.

References

1. Z. Zheng and A. Weiner, "Spectral phase correlation of coded femtosecond pulses by second-harmonic generation in thick nonlinear crystals," Opt. Lett. **25**(13), 984–986 (2000).
2. Z. Zheng, A. Weiner, K. Parameswaran, *et al.*, "Low-power spectral phase correlator using periodically poled linbo 3 waveguides," IEEE Photonics Technol. Lett. **13**(4), 376–378 (2001).
3. J. M. Lukens, A. Dezfooliyan, C. Langrock, *et al.*, "Orthogonal spectral coding of entangled photons," Phys. Rev. Lett. **112**(13), 133602 (2014).
4. M. J. Padgett and R. W. Boyd, "An introduction to ghost imaging: quantum and classical," Phil. Trans. R. Soc. A. **375**(2099), 20160233 (2017).

Optics EXPRESS

5. G. B. Lemos, V. Borish, G. D. Cole, *et al.*, "Quantum imaging with undetected photons," Nature **512**(7515), 409–412 (2014).
6. A. F. Abouraddy, B. E. A. Saleh, A. V. Sergienko, *et al.*, "Role of entanglement in two-photon imaging," Phys. Rev. Lett. **87**(12), 123602 (2001).
7. C. Bonato, A. V. Sergienko, B. E. A. Saleh, *et al.*, "Even-order aberration cancellation in quantum interferometry," Phys. Rev. Lett. **101**(23), 233603 (2008).
8. L. A. P. Filpi, M. V. da Cunha Pereira, and C. H. Monken, "Experimental observation of aberration cancellation in entangled two-photon beams," Opt. Express **23**(4), 3841–3850 (2015).
9. A. N. Black, E. Giese, B. Braverman, *et al.*, "Quantum nonlocal aberration cancellation," Phys. Rev. Lett. **123**(14), 143603 (2019).
10. M. Liscidini and J. Sipe, "Stimulated emission tomography," Phys. Rev. Lett. **111**(19), 193602 (2013).
11. M. A. Ciampini, A. Geraldi, V. Cimini, *et al.*, "Stimulated emission tomography: beyond polarization," Opt. Lett. **44**(1), 41–44 (2019).
12. J. Rocha, D. Pires, J. Neto, *et al.*, "Speckle filtering through nonlinear wave mixing," Opt. Lett. **46**(16), 3905–3908 (2021).
13. B. P. da Silva, G. dos Santos, A. de Oliveira, *et al.*, "Observation of a triangular-lattice pattern in nonlinear wave mixing with optical vortices," Optica **9**(8), 908–912 (2022).
14. R. W. Boyd, A. L. Gaeta, and E. Giese, "Nonlinear optics," in *Springer Handbook of Atomic, Molecular, and Optical Physics*, (Springer, 2008), pp. 1097–1110.
15. P. S. Ribeiro, D. Caetano, M. Almeida, *et al.*, "Observation of image transfer and phase conjugation in stimulated down-conversion," Phys. Rev. Lett. **87**(13), 133602 (2001).
16. R. Keys, "Cubic convolution interpolation for digital image processing," IEEE Trans. Acoust., Speech, Signal Process. **29**(6), 1153–1160 (1981).
17. J. Wang and N. Zheng, "A novel fractal image compression scheme with block classification and sorting based on pearson's correlation coefficient," IEEE Trans. Image Process. **22**(9), 3690–3702 (2013).
18. S. Mohapatra and J. C. Weisshaar, "Modified pearson correlation coefficient for two-color imaging in spherocylindrical cells," BMC Bioinf. **19**(1), 428 (2018).
19. A. Barh, P. J. Rodrigo, L. Meng, *et al.*, "Parametric upconversion imaging and its applications," Adv. Opt. Photonics **11**(4), 952–1019 (2019).
20. R. S. Aspden, N. R. Gemmell, P. A. Morris, *et al.*, "Photon-sparse microscopy: visible light imaging using infrared illumination," Optica **2**(12), 1049–1052 (2015).
21. F. Wang, D. Banerjee, Y. Liu, *et al.*, "Upconversion nanoparticles in biological labeling, imaging, and therapy," Analyst **135**(8), 1839–1854 (2010).
22. X. Wu, G. Chen, J. Shen, *et al.*, "Upconversion nanoparticles: a versatile solution to multiscale biological imaging," Bioconjugate Chem. **26**(2), 166–175 (2015).
23. P. Manurkar, N. Jain, M. Silver, *et al.*, "Multidimensional mode-separable frequency conversion for high-speed quantum communication," Optica **3**(12), 1300–1307 (2016).